Coupled Systems Mechanics, *Vol. 8, No. 2 (2019) 129–146*
DOI: https://doi.org/10.12989/csm.2019.8.2.129

Numerical simulation of single-phase two-components flow in naturally fractured oil reservoirs

João Gabriel Souza Debossam*, Juan Diego dos Santos Heringer, Grazione de Souza and Helio Pedro Amaral Souto

Polytechnic Institute, Rio de Janeiro State University, Rua Bonfim 25, Vila Amelia, 28625-570, Nova Friburgo, Rio de Janeiro, Brazil

(Received September 28, 2018, Revised December 19, 2018, Accepted December 20, 2018)

Abstract. The main goal of this work is to develop a numerical simulator to study an isothermal single-phase two-component flow in a naturally fractured oil reservoir, taking into account advection and diffusion effects. We use the Peng-Robinson equation of state with a volume translation to evaluate the properties of the components, and the discretization of the governing partial differential equations is carried out using the Finite Difference Method, along with implicit and first-order upwind schemes. This process leads to a coupled non-linear algebraic system for the unknowns pressure and molar fractions. After a linearization and the use of an operator splitting, the Conjugate Gradient and Bi-conjugated Gradient Stabilized methods are then used to solve two algebraic subsystems, one for the pressure and another for the molar fraction. We studied the effects of fractures in both the flow field and mass transport, as well as in computing time, and the results show that the fractures affect, as expected, the flow creating a thin preferential path for the mass transport.

Keywords: compositional simulation; equation of state; operator splitting; finite difference method; fractured oil reservoir

1. Introduction

Porous media flow occurs in many engineering problems, for example, aquifer contamination and water transport (de Borst, Réthoré and Abellan 2006, Li 2017), carbon sequestration (Das and Dutta 2017), membrane filtration (Hanspal *et al.* 2009), chemical processes (Anca-Couce, Zobel and Jakobsen 2013) and hydrocarbons recovery (Zaydullin *et al.* 2014, Wu and Sun 2016). In the oil and gas industry, since the 1960s, porous media flow, reservoir management, wellbore pressure profile and reservoir characterization have been studied using numerical reservoir simulation. Numerical methods have been used to maximize hydrocarbon recovery, aiming to obtain an optimized wellbore control. In this context, there are still many issues involving transport phenomena in heterogeneous reservoirs (Jmili, Wilhite and Green 2011, Biryukov and Kuchuk 2012, Mendes, Murad and Pereira 2012).

*Corresponding author, E-mail: jdebossam@iprj.uerj.br

http://www.techno-press.org/?journal=csm&subpage=8 ISSN: 2234-2184(Print), 2234-2192(Online)

Indeed, physical-mathematical modeling and numerical simulations of flow in heterogeneous porous media have attracted the attention of researchers in the past decades. Porous media flow in naturally fractured reservoirs (NFRs) is of particular interest (Nelson 2001, Wang 2013, Jiang and Younis 2015, Nikolic, Ibrahimbegovic and Miscevic 2016, Cavalcante Filho and Sepehrnoori 2017). In these rock formations, there are permeability field, k, and porosity field, ϕ, with high contrasts in their values (Zidane and Firoozabadi 2017) caused by geological factors. A natural fracture is a planar discontinuity (Hadzalic, Ibrahimbegovic and Dolarevic 2018, Hadzalic, Ibrahimbegovic and Nikolic 2018) in reservoir rock due to deformation or diagenesis (chemical and physical changes after deposition) (Tiab and Donaldson 2004). Cavities, called vugs, can also be formed depending on the scale of the heterogeneities and on their spatial distribution. High permeability channels, natural fractures and vugs in carbonates, for instance, are the result of the dissolution of rocks.

Matrix and fractures, considered as two different regions, must be used to model fluid flow in NFRs (Lee, Lough and Jensen 2001). In the porous matrix (rock), a fracture or a fracture network may exist. In general, fractures have much greater permeabilities and porosities than the porous matrix. Depending on the reservoir characteristics (Nelson 2001):

1. fractures provide the essential reservoir permeability and porosity;
2. fractures give only the essential reservoir permeability;
3. fractures have a secondary role for permeability; or
4. fractures have influence only on the reservoir anisotropy.

Fig. 1 shows schematically a naturally fractured reservoir. Different approaches can be considered depending on the hypothesis adopted to model fluid storage, and matrix and fracture flows:

1. double porosity, double permeability;
2. Multiple Interacting Continua (MINC);
3. Embedded Fracture Modeling (EFM); and
4. Discrete Fracture Networks (DFN).

In this work, we use a discrete network of fractures. Thus, a computational grid is employed to represent the geometry of each fracture (Secchi and Schrefler 2012).

For an accurate simulation of the flow in the reservoir, as we use a discrete network of fractures, a large number of grid blocks are necessary near the fractures. As a consequence, we have an increase in computing time (Moinfar 2013). Another complexity appears since we are interested in the study of the displacement of two components in a single-phase flow, which is a version of a compositional model (Chen 2007). Therefore, due to difficulties arising from the heterogeneity (fractures) and the compositional model (Hoteit and Firoozabadi 2006, Geiger, Schmid and Zaretskiy 2017), a large CPU time is expected. The more heterogeneous is the reservoir (depending on fracture properties and positions), the greater the computational effort.

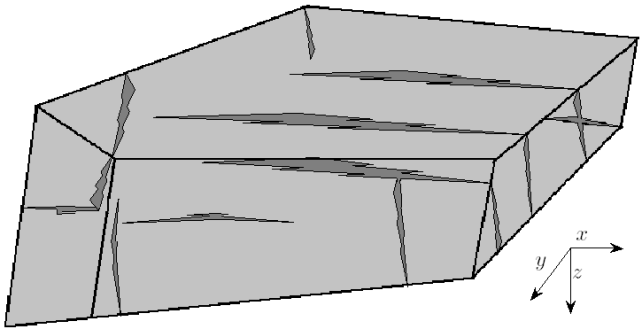

Fig. 1 Naturally fractured reservoir: fractures in dark gray color and matrix in light gray color

2. Governing equations and equation of state

Here, we are interested in a numerical simulation of an isothermal single-phase two-component flow in a naturally fractured oil reservoir considering advection and diffusion effects. The governing equations are obtained from continuity equation, Darcy's law and rock and fluid properties (Lewis and Schrefler 1998, Chen 2007). Thus, we have the following Partial Differential Equation (PDE) for pressure,

$$\frac{\partial}{\partial t}\left(\phi\xi\right) = \nabla\cdot\left[\frac{\xi}{\mu}\mathbf{k}\left(\nabla p - \gamma\nabla z\right)\right] + q, \tag{1}$$

where p is the pressure, ϕ is the porosity, ξ is the molar density, μ is the fluid viscosity, $\mathbf{k}$ is the absolute rock permeability tensor, γ is the product of density and gravity magnitude, z is the depth and q a source term. On the other hand, for molar fractions,

$$\frac{\partial}{\partial t}\left(\phi x_m\xi\right) = \nabla\cdot\left[\frac{x_m\xi}{\mu}\mathbf{k}\left(\nabla p - \gamma\nabla z\right) + \phi\xi\mathbf{D}_m\nabla x_m\right] + q_m \qquad m = 1, 2, \ldots, N_c, \tag{2}$$

where x_m is the molar fraction, q_m is a source term, N_c is the number of components and $\mathbf{D}_m$ is the effective dispersion tensor. In three dimensions, this tensor is defined by (Chen 2007)

$$\mathbf{D}_i\left(\mathbf{u}\right) = d_{im}\mathbf{I} + \left|\mathbf{u}\right|\left(d_{il}\mathbf{E}\left(\mathbf{u}\right) + d_{it}\mathbf{E}^{\perp}\left(\mathbf{u}\right)\right), \tag{3}$$

where d_{im} is the molecular diffusion coefficient, d_{it} and d_{il} are the transverse and longitudinal dispersion coefficients, $\mathbf{u}$ is the Darcy's velocity, and $\mathbf{E}\left(\mathbf{u}\right)$ is the orthogonal projection and $\mathbf{E}^{\perp}\left(\mathbf{u}\right) = \mathbf{I} - \mathbf{E}\left(\mathbf{u}\right)$, where $\mathbf{I}$ is the identity matrix.

Therefore, we must solve numerically Eq. (1) for the fluid phase and Eq. (2) for one component. We use the Peng-Robinson equation of state (PR-EoS) with a volume translation to evaluate the properties of the components. As the molar density is a function of the compressibility factor Z, we have

$$\xi = \frac{p}{RTZ}, \tag{4}$$

where R is the universal gas constant, and the Peng-Robinson cubic equation can be written as

$$Z^3 - (1 - B) Z^2 + \left(A - 2B - 3B^2\right) Z - \left(AB - B^2 - B^3\right) = 0, \tag{5}$$

where A and B are parameters that are functions of the critical temperature and pressure of the components.

Eq. (5) is a cubic polynomial and has three roots. When there is only one real root, then it is chosen. With three real roots, we choose the largest root for gas flow, while we choose the smallest for oil flow (Wu and Sun 2016). Some parameters of the equation of state are specific for vapor pressure. Thus, for liquids, we apply a volume translation to avoid errors (Chen 2007),

$$v_{corr} = v_{EoS} + C, \tag{6}$$

where the volume v is the reciprocal of the molar density ξ, and C is the correction factor. This factor is computed using the temperature and component's properties, as discussed by Hoyos (2004).

3. Numerical methodology

A numerical method is necessary to solve the partial differential equations considered here, so the discretization of the PDEs is performed using the Finite Difference Method (FDM), and we use a block-centered grid, an implicit time formulation, central differences for the diffusive terms and a first-order upwind scheme for the advective terms. Discrete fracture networks are placed in the computational grid, considering planar fractures distributed in a structured mesh. To better represent and simulate the fractures, which are very small, a logarithmic grid refinement is used near the fracture to make the mesh size small enough (Souza and Amaral Souto 2016).

Considering a diagonal permeability tensor $\mathbf{k}$ and a diagonal diffusion tensor $\mathbf{D}_m$ (Chen 2007), and adopting the notation $f\left(x_i, t^n\right) = f_i^n$, the discrete form of Eqs. (1) and (2) are

$$\begin{aligned}
&\mathbb{T}^{n+1}_{x,i+1/2,j,k}\left(p^{n+1}_{i+1,j,k} - p^{n+1}_{i,j,k}\right) - \mathbb{T}^{n+1}_{x,i-1/2,j,k}\left(p^{n+1}_{i,j,k} - p^{n+1}_{i-1,j,k}\right) \\
&+\mathbb{T}^{n+1}_{y,i,j+1/2,k}\left(p^{n+1}_{i,j+1,k} - p^{n+1}_{i,j,k}\right) - \mathbb{T}^{n+1}_{y,i,j-1/2,k}\left(p^{n+1}_{i,j,k} - p^{n+1}_{i,j-1,k}\right) \\
&+\mathbb{T}^{n+1}_{z,i,j,k+1/2}\left(p^{n+1}_{i,j,k+1} - p^{n+1}_{i,j,k}\right) - \mathbb{T}^{n+1}_{z,i,j,k-1/2}\left(p^{n+1}_{i,j,k} - p^{n+1}_{i,j,k-1}\right) \\
&- (\mathbb{T}\gamma)^{n+1}_{x,i+1/2,j,k}\left(z_{i+1,j,k} - z_{i,j,k}\right) + (\mathbb{T}\gamma)^{n+1}_{x,i-1/2,j,k}\left(z_{i,j,k} - z_{i-1,j,k}\right) \\
&- (\mathbb{T}\gamma)^{n+1}_{y,i,j+1/2,k}\left(z_{i,j+1,k} - z_{i,j,k}\right) + (\mathbb{T}\gamma)^{n+1}_{y,i,j-1/2,k}\left(z_{i,j,k} - z_{i,j-1,k}\right) \\
&- (\mathbb{T}\gamma)^{n+1}_{z,i,j,k+1/2}\left(z_{i,j,k+1} - z_{i,j,k}\right) + (\mathbb{T}\gamma)^{n+1}_{z,i,j,k-1/2}\left(z_{i,j,k} - z_{i,j,k-1}\right)
\end{aligned}$$

$$+Q_{i,j,k}^{n+1} = \left[V_b c \left(p^{n+1} \right) \frac{p^{n+1} - p^n}{\Delta t} \right]_{i,j,k}, \tag{7}$$

where the pressure in the new time level p^{n+1} is the unknown value, and

$$\begin{aligned}
&\mathbb{D}_{mx,i+1/2,j,k}^{n+1} \left(x_{m,i+1,j,k}^{n+1} - x_{m,i,j,k}^{n+1} \right) - \mathbb{D}_{mx,i-1/2,j,k}^{n+1} \left(x_{m,i,j,k}^{n+1} - x_{m,i-1,j,k}^{n+1} \right) \\
&+\mathbb{D}_{my,i,j+1/2,k}^{n+1} \left(x_{m,i,j+1,k}^{n+1} - x_{m,i,j,k}^{n+1} \right) - \mathbb{D}_{my,i,j-1/2,k}^{n+1} \left(x_{m,i,j,k}^{n+1} - x_{m,i,j-1,k}^{n+1} \right) \\
&+\mathbb{D}_{mz,i,j,k+1/2}^{n+1} \left(x_{m,i,j,k+1}^{n+1} - x_{m,i,j,k}^{n+1} \right) - \mathbb{D}_{mz,i,j,k-1/2}^{n+1} \left(x_{m,i,j,k}^{n+1} - x_{m,i,j,k-1}^{n+1} \right) \\
&+ \left(x_m \mathbb{T} \right)_{x,i+1/2,j,k}^{n+1} \left(p_{i+1,j,k}^{n+1} - p_{i,j,k}^{n+1} \right) - \left(x_m \mathbb{T} \right)_{x,i-1/2,j,k}^{n+1} \left(p_{i,j,k}^{n+1} - p_{i-1,j,k}^{n+1} \right) \\
&+ \left(x_m \mathbb{T} \right)_{y,i,j+1/2,k}^{n+1} \left(p_{i,j+1,k}^{n+1} - p_{i,j,k}^{n+1} \right) - \left(x_m \mathbb{T} \right)_{y,i,j-1/2,k}^{n+1} \left(p_{i,j,k}^{n+1} - p_{i,j-1,k}^{n+1} \right) \\
&+ \left(x_m \mathbb{T} \right)_{z,i,j,k+1/2}^{n+1} \left(p_{i,j,k+1}^{n+1} - p_{i,j,k}^{n+1} \right) - \left(x_m \mathbb{T} \right)_{z,i,j-1/2,k}^{n+1} \left(p_{i,j,k}^{n+1} - p_{i,j,k-1}^{n+1} \right) \\
&- \left(\mathbb{T}_m \gamma \right)_{x,i+1/2,j,k}^{n+1} \left(z_{i+1,j,k} - z_{i,j,k} \right) + \left(\mathbb{T}_m \gamma \right)_{x,i-1/2,j,k}^{n+1} \left(z_{i,j,k} - z_{i-1,j,k} \right) \\
&- \left(\mathbb{T}_m \gamma \right)_{y,i,j+1/2,k}^{n+1} \left(z_{i,j+1,k} - z_{i,j,k} \right) + \left(\mathbb{T}_m \gamma \right)_{y,i,j-1/2,k}^{n+1} \left(z_{i,j,k} - z_{i,j-1,k} \right) \\
&- \left(\mathbb{T}_m \gamma \right)_{z,i,j,k+1/2}^{n+1} \left(z_{i,j,k+1} - z_{i,j,k} \right) + \left(\mathbb{T}_m \gamma \right)_{z,i,j,k-1/2}^{n+1} \left(z_{i,j,k} - z_{i,j,k-1} \right) \\
&+Q_{m,i,j,k}^{n+1} = \left[V_b \frac{\left(\phi x_m \xi \right)^{n+1} - \left(\phi x_m \xi \right)^n}{\Delta t} \right]_{i,j,k}, \qquad m = 1, 2, \ldots, N_c - 1,
\end{aligned} \tag{8}$$

where the new molar fraction x_m^{n+1} is the unknown. Here $Q_{m,i,j,k} = V_{b_{i,j,k}} q_{m,i,j,k}$, $Q_{i,j,k} = V_{b_{i,j,k}} q_{i,j,k}$, $V_{b_{i,j,k}} = (\Delta x \Delta y \Delta z)_{i,j,k}$, where $\Delta x_{i,j,k}$, $\Delta y_{i,j,k}$ and $\Delta z_{i,j,k}$ are the grid sizes in the x-, y- and z-directions. Also, $\mathbb{T}$ is known as the transmissibility and is defined as

$$\mathbb{T}_{x,i\pm\frac{1}{2},j,k}^{n+1} \equiv \left(\frac{\xi k_{xx} A_x}{\mu \Delta x} \right)_{i\pm\frac{1}{2},j,k}^{n+1}, \tag{9}$$

and $\mathbb{T}_m = x_m \mathbb{T}$. A similar definition is used for the other directions. The dispersion coefficients are given by

$$\mathbb{D}_{mx,i\pm1/2} \equiv \left(\frac{A_x \phi \xi D_{mx}}{\Delta x} \right)_{i\pm1/2}, \tag{10}$$

and it is defined in a similar way for the other two directions.

We also use an operator splitting technique (Vennemo 2016) along with a linearization such as we solve pressure and molar fraction equations into two separated discrete subsystems. This procedure leads to a coupled linear system for the unknown pressure and molar fractions. We apply the Conjugate Gradient Method (CG) to solve the pressure equation (symmetric coefficient matrix) and the Bi-Conjugated Gradient Stabilized Method (BiCG) for the molar fraction equation (asymmetric coefficient matrix) (Saad 2003).

The process steps to calculate the unknowns at time $n + 1$ are described below:

1. given the pressure p and the molar fraction x_m, the fluid properties are evaluated with the Peng-Robinson EoS;
2. we solve Eq. (7) for the pressure with the CG method;
3. then we solve Eq. (8) for the molar fraction with the BiCG method;
4. iterate until convergence is achieved;

and these steps are illustrated in the flowchart seen in Fig. 2. We must emphasize that, as reported in Maes (2016), decoupling the equations introduce an additional error (compared to a fully implicit method), and we can not use large increments of time if we want to preserve the accuracy of the results.

4. Numerical simulations

In this section, we present our numerical results for simulations of a compositional flow through a fractured reservoir. The reservoir is of size 400 m $\times$ 200 m $\times$ 50 m, and pressure is prescribed in both west and east sides (30,000 kPa and 20,000 kPa, respectively), and there is no mass flux through the other boundaries. In the west boundary, a heavier component is flowing into the reservoir with a molar fraction equal to 1, and we keep a constant temperature of 300 K. All simulations were run on a Dell PowerEdge T620 with two Intel Xeon Processor E5-2620 (2 GHz) and 16 GB of memory.

First of all, we study the grid dependence of the results. As expected, the first-order upwind scheme introduces a numerical diffusion, and it is minimized using a more refined mesh. In Fig. 3, we see how the mesh size affects the results. As the number of cell blocks increases, the molar fraction behavior indicates that the results are converging to the same values. We also realize that the computational time for the 320 cells mesh is higher than double the time for 160 cells, and the results are practically the same. Therefore, all the other simulations were carried out using 160 cells in the x-direction and 5 in z-direction. In y-direction, we apply a logarithmic grid refinement around the fractures, resulting in 164 cells. For all simulations, we neglected hydraulic dispersion and gravity effects.

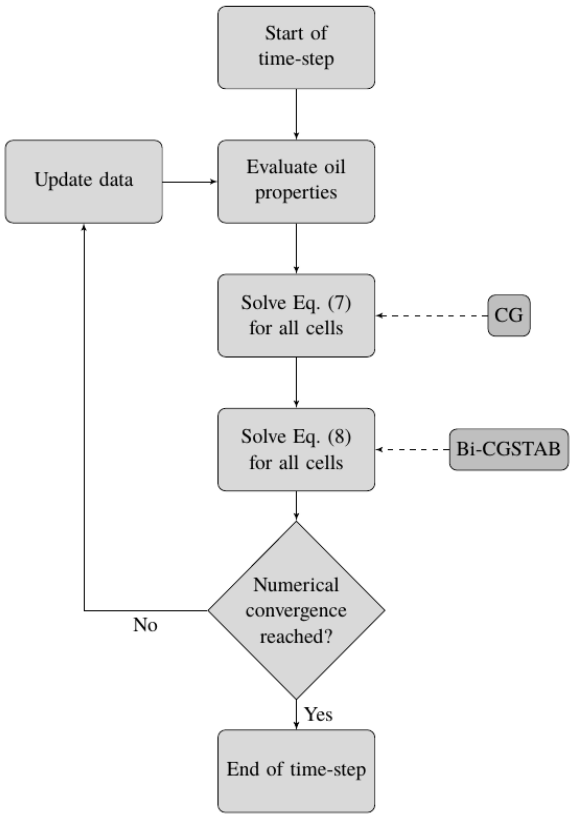

Fig. 2 Flowchart of a single simulation time-step

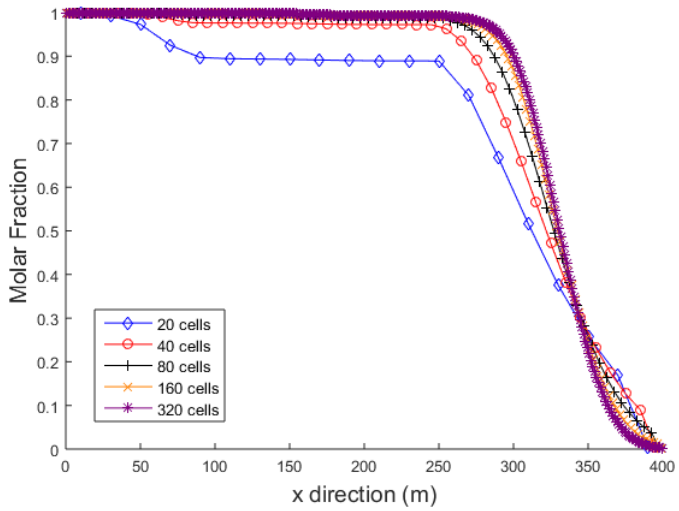

Fig. 3 Profile of the molar fraction for different meshes

4.1 First example

The properties of the reservoir and fractures, for the first example, can be seen in Table 1. The fracture permeability is four thousand times greater than in the matrix, and the porosity is four times greater in the fracture.

Table 1 Properties of the reservoir for the first example

Parameter	Symbol	Value	Unit
Porosity (matrix)	ϕ_m	0.2	-
Permeability (matrix)	k_m	5	mD
Porosity (fracture)	ϕ_f	0.8	-
Permeability (fracture)	k_f	20×10^3	mD
Initial pressure	p_{init}	25×10^3	kPa

The first example considers the flow in a reservoir containing four fractures. All fractures are placed at the same x coordinate, equal to 30 m, and have the same length of 200 m and aperture of 25 cm. This information is summed up in Table 2. Here l_x is the length in x-direction, and x_0 and y_0 are the coordinates of the first vertex of the fractures. The height of the planar fractures coincides with that of the reservoir (50 m). The spatial distribution of fractures can be seen in Fig. 4.

Table 2 Location of fractures

Parameter	Fracture 1	Fracture 2	Fracture 3	Fracture 4
l_x (m)	200	200	200	200
x_0 (m)	50	50	50	50
y_0 (m)	25	75	125	175

The molar fraction of the entering liquid after 750 days is shown in Fig. 5. Four cases were considered:

1. default case (Table 1);
2. ϕ_m=0.2, ϕ_f=0.2, k_m=5 mD and k_f=20 D;
3. ϕ_m=0.2, ϕ_f=0.8, k_m=5 mD and k_f=200 D; and
4. ϕ_m=0.2, ϕ_f=0.8, k_m=5 mD and k_f=2 D.

When compared to the default case, as showed in Fig. 5, a porosity of 20% in the fracture (Case 2) does not change significantly the flow behavior. It seems reasonable since fractures are narrow channels and cannot store a large amount of mass. The effective mass transport increases through the fractures for a greater permeability (Case 3), but the difference is not significant. Otherwise, for a lower permeability (Case 4), it can be seen that we have less mass concentrated at the end of the fractures, and the impact on the molar fraction distribution is substantial.

In Fig. 6, we present the results of the numerical simulation of the flow through the fractured reservoir as the time progresses, and we can find the molar fraction field for 150, 400, 700 and 1,000 days. According to expectation, the flow is slower into the matrix compared to that into the fractures,

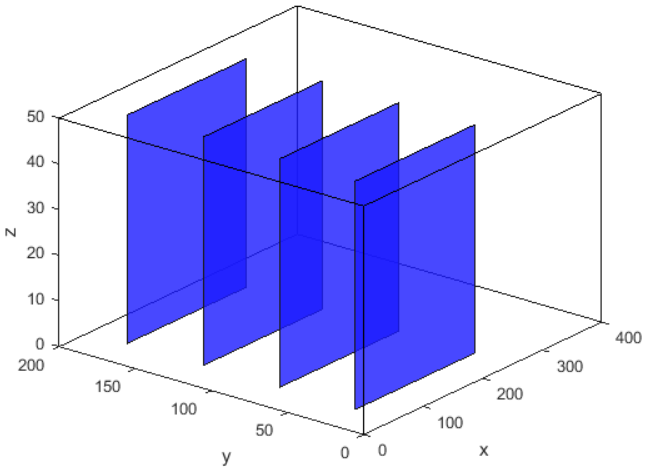

Fig. 4 Fractures arrangement for the first example

and it travels a shorter distance into the matrix for the same time interval. We can also see in Fig. 6 how the presence of the fractures causes a greater heterogeneity on the molar fraction field.

4.2 Second example

A second example is introduced to study how the matrix-fracture interaction is affected by the rock properties. In Fig. 7 is depicted the molar fraction distribution, also for a reservoir containing four fractures with the same length, but now with an aperture of 2.5 cm (in contrast to the 25 cm of the first example). For this example we also change the permeabilities and porosity, so we have: ϕ_m=0.2, ϕ_f=0.6, k_m=20 mD and k_f=50$\times 10^3$ mD.

After comparing the results found in Figs. 5 and 7, taking into account the time differences (300 days versus 750 days of the previous example), we realize how the permeability of the matrix affects the velocity of the flow, since the flow front is more advanced even for a shorter time. As a consequence of the greater permeability value, the flow velocity is higher (according to Darcy's law) than the corresponding flow velocity in Fig. 5. We can also observe in Fig. 7, as in previous cases, a mass transport along the y-direction due to the increase in pressure inside the fractures (Fig. 8).

In the following, using the same properties of this example, we address the influence of the mesh refinement around the fractures. Therefore, in addition to the already used 164 cells in y-direction, we tested meshes with 44, 84 and 324 cells. The corresponding results for the molar fraction are in Fig. 9. As expected, we obtain more accurate results and depiction of the fractures with the more refined meshes. However, it demands more CPU effort.

4.3 Third example

The last example is similar to the previous one, but now the initial vertices of the fractures do not have the same coordinates, and they have different lengths, porosities, and permeabilities, although

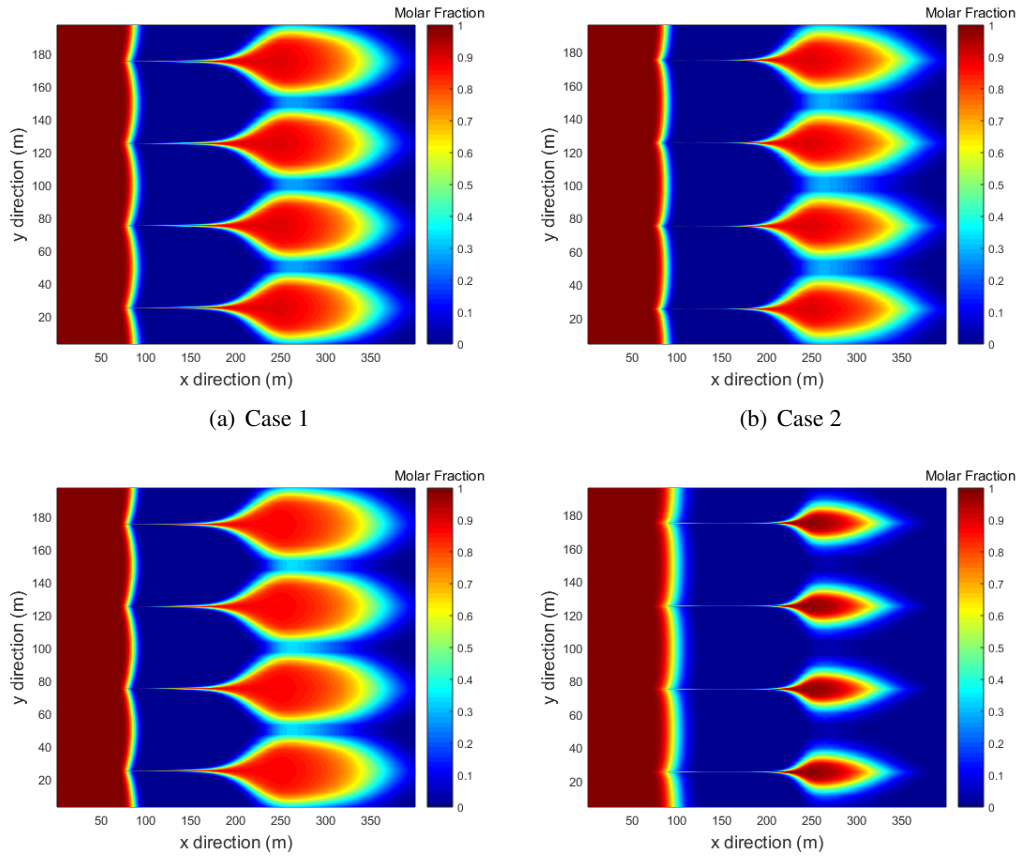

(a) Case 1 (b) Case 2

(c) Case 3 (d) Case 4

Fig. 5 Molar fraction for 750 days

they have the same aperture of 2.5 cm. Table 3 shows the fractures lengths, vertices and properties. The new spatial arrangement of the fractures is illustrated in Fig. 10.

Table 3 Location of fractures and properties

Parameter	Fracture 1	Fracture 2	Fracture 3	Fracture 4
l_x (m)	100	70	120	200
x_0 (m)	30	180	80	40
y_0 (m)	35	135	85	175
k_f (D)	25	100	50	35
ϕ_f	0.5	0.8	0.6	0.6

Fig. 11 shows the molar fraction after 100, 150, 200 and 300 days of simulation. From the observation of Figs. 5 and 11 we can see that they are very different, showing how the fractures position and properties can drastically alter the molar fraction distribution.

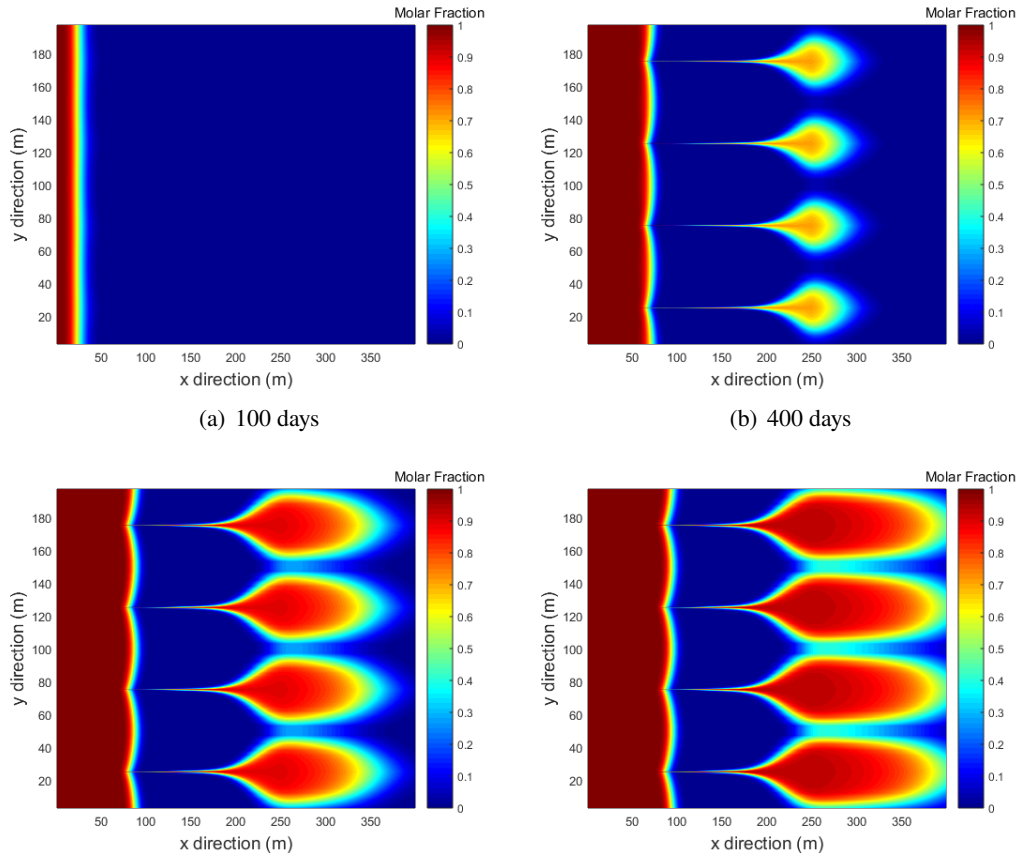

(a) 100 days (b) 400 days

(c) 700 days (d) 1,000 days

Fig. 6 Molar fraction as a function of time

It is also worth mentioning that the CPU time for this non-regular fracture positioning was significantly higher (more than double the time) compared with the case when the first vertices of the fractures were all in the same position, and they had the same properties. This fact demonstrates that the distribution and properties of fractures play an important role in the complexity of flow and mass transfer.

4.4 Strategy to reduce computing time

To investigate the influence of the presence of fractures on computing time, we performed a simulation with no fractures at all, but with the same number of cells as for the first example. For this case, the simulation time was 23 hours, 17 minutes and 47 seconds. On the other hand, the same simulation with the regular arrangement of fractures took 32 hours, 50 minutes and 13 seconds. Lastly, for the irregular arrangement (third example), the simulation ended after 67 hours, 27 minutes and 22 seconds. Therefore, the more disordered is the arrangement of fractures (as in a real reservoir),

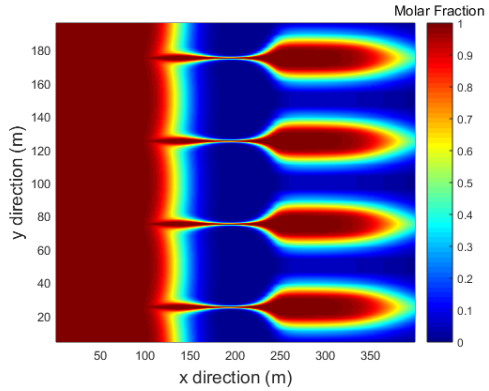

Fig. 7 Molar fraction for the second example

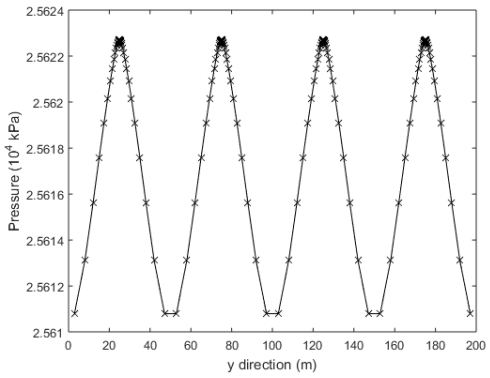

Fig. 8 Pressure along the y-direction

the more demanding will be the simulations, which shows the difficulties of simulating real cases.

In this work, we adopted a strategy to reduce the CPU time consisting of using different time steps for the numerical solution of pressure and molar fraction equations. Considering the same properties as those employed in the second example, we kept a fixed time-step when solving the molar fraction equation, while performing simulations to determine the pressure with time-steps two, five, ten and twenty times greater than that of the simulation of the molar fraction equation.

To be sure that this strategy does not result in less accurate results, Fig. 12 contains a plot of the absolute relative difference between the molar faction values, determined with the different time-steps for pressure calculations, taking as reference the values obtained in the second example, Fig 7. For time-steps smaller than five times that used to calculate the molar fraction the relative difference is very small, and we can consider that values are accurate. However, for the 10:1 and 20:1 ratios we note, mainly near the fractures, that the molar fraction values start to become very different.

Table 4 shows the time of simulation and the Number of Intermediate Steps (NIS). When NIS is one, we have the default case, where the time-steps used to solve pressure and molar faction equations

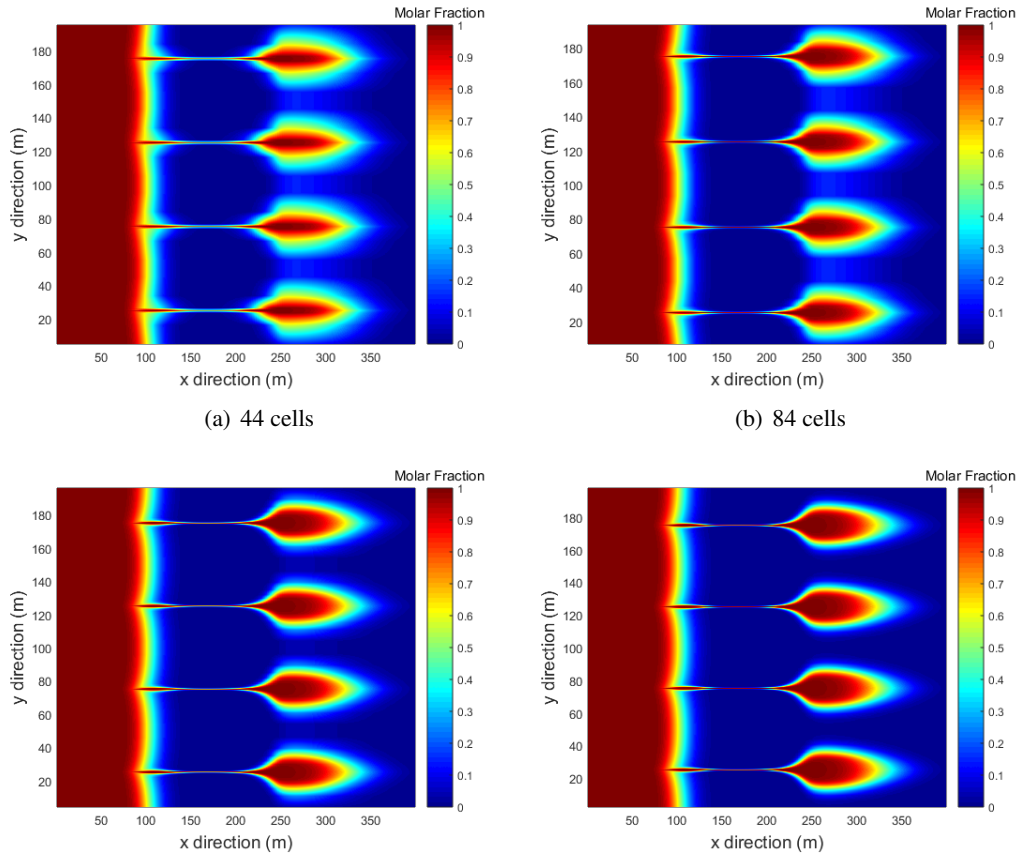

(a) 44 cells (b) 84 cells

(c) 164 cells (d) 324 cells

Fig. 9 Molar fraction for different meshes

are the same. We can also see that the total execution time reduction grows as we increase the time-step ratios. However, this reduction is accompanied by an increase in the deviation from the default case values for the molar fraction. Nevertheless, when we use a 5:1 time-step ratio we achieve a reduction of approximately 14% of CPU time and the results are practically the same, making it a good choice.

Table 4 Total simulation time

NIS	Total Simulation Time	Time Variation
1	32h 50min 13s	–
2	37h 04min 02s	+12.9%
5	28h 21min 41s	-13.6%
10	25h 15min 40s	-23.1%
20	24h 30min 55s	-25.3%

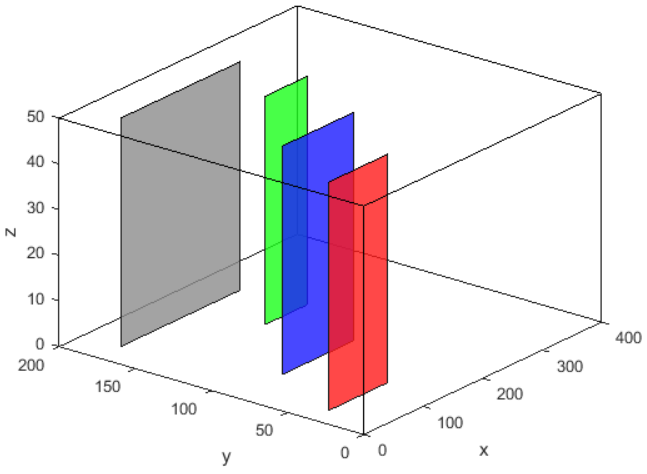

Fig. 10 Fractures arrangement for the third example

5. Conclusions

In this paper, we addressed reservoir simulation of a naturally fractured reservoir considering only planar fractures. The finite difference method and an implicit formulation were used to obtain a numerical solution for a single-phase two-component flow. The methodology employed was able to adequately capture the effects due to fractures, as well as the advection-diffusion mass transport on compositional flow. Also, we successfully implemented the operator splitting technique and the grid refinement around the fractures, although from a computational point of view they are very costly in computing time.

As expected, the additional complexity resulting from the introduction of fractures leads to an increase in computational time. Furthermore, when the fractures were irregularly arranged in the reservoir, the CPU time increased even more. Thus, the arrangement of fractures is of great importance in the total execution time. The more irregular the distribution of fractures and the more their properties are different, the longer the execution time will be.

Using different time-steps to solve pressure and molar fraction equations result in an effective strategy for solving this problem since, for an appropriate choice, it reduced simulation time by about 14% while keeping the precision of the results. Therefore, as we verified, the use of an operator splitting method enabled the use of different time increments to obtain the pressure and molar concentration, similar to what is done in some versions of the IMPES (Implicit Pressure Explicit Saturation) method (Chen 2007). However, due to the errors introduced by decoupling the equations (Maes 2016), a detailed numerical study must be done to maintain the accuracy of the results.

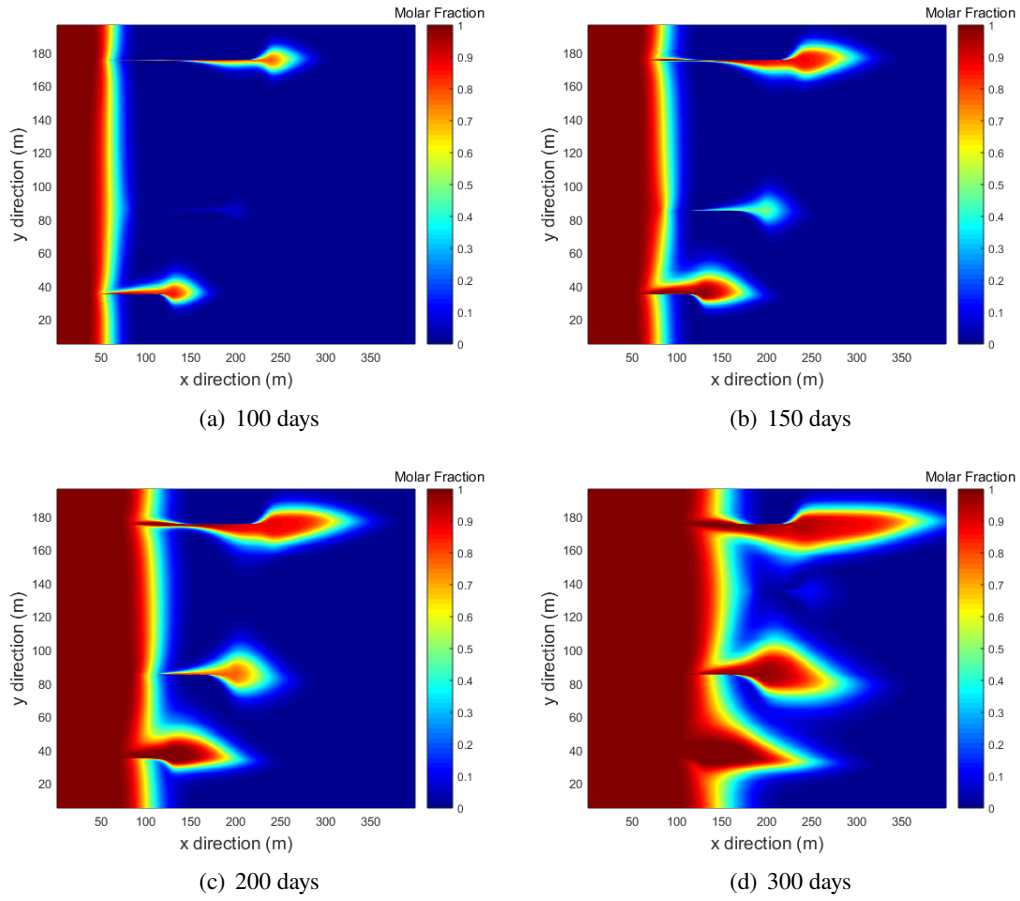

(a) 100 days (b) 150 days

(c) 200 days (d) 300 days

Fig. 11 Molar fraction for an irregular distribution of fractures

Acknowledgements

The authors gratefully thanks Rio de Janeiro State University, Coordination for the Improvement of Higher Education Personnel (CAPES) - Finance Code 001, and National Council for Scientific and Technological Development (CNPq) for their support.

References

Anca-Couce, A., Zobel, N. and Jakobsen, H.A. (2013), "Multi-scale modeling of fixed-bed thermo-chemical processes of biomass with the representative particle model: Application to pyrolysis", *Fuel*, **103**, 773-782.

Biryukov, D. and Kuchuk, F.J. (2012), "Transient pressure behavior of reservoirs with discrete conductive faults and fractures", *Transp. Por. Med.*, **95**(1), 239-268.

Cavalcante Filho, J.S.A. and Sepehrnoori, K. (2017), "Simulation of planar hydraulic fractures with variable conductivity using the embedded discrete fracture model", *J. Petrol. Sci. Eng.*, **153**, 212-222.

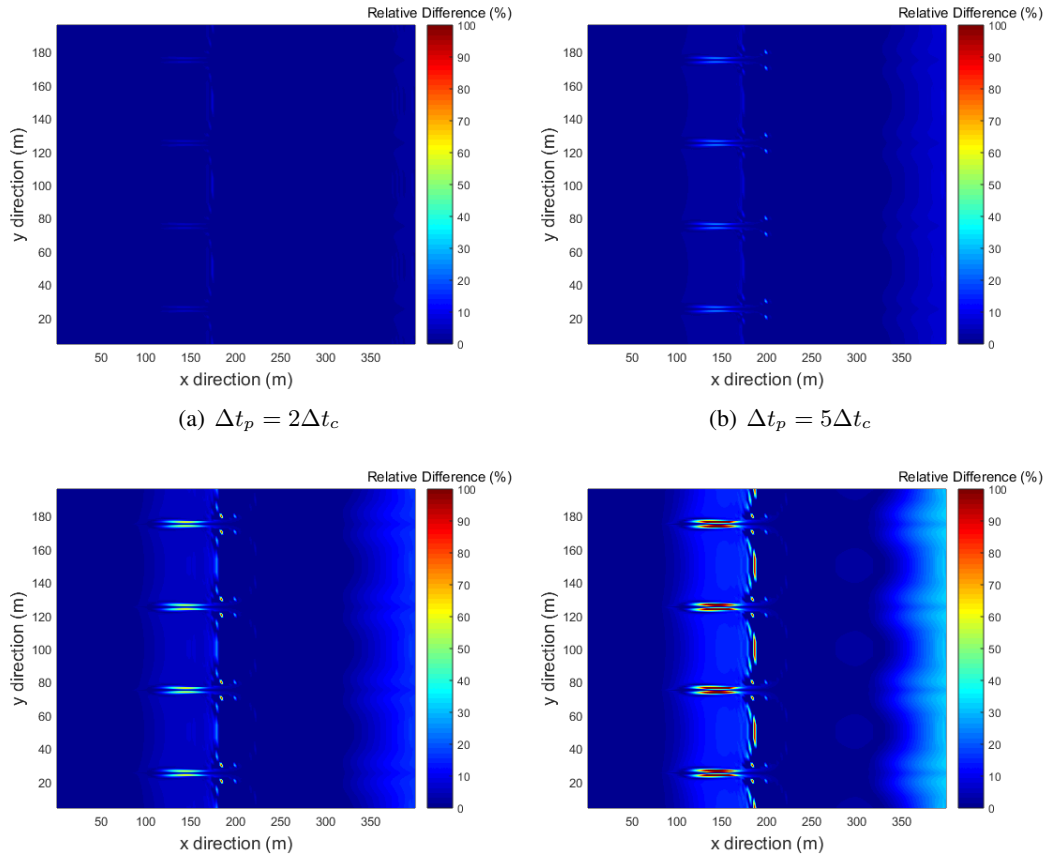

(a) $\Delta t_p = 2\Delta t_c$ (b) $\Delta t_p = 5\Delta t_c$

(c) $\Delta t_p = 10\Delta t_c$ (d) $\Delta t_p = 20\Delta t_c$

Fig. 12 Molar fraction for an irregular distribution of fractures

Chen, Z. (2007) *Reservoir Simulation-Mathematical Techniques in Oil Recovery*, Society of Industrial and Applied Mathematics, Philadelphia, Pennsylvania, U.S.A.

Das, S. and Dutta, P. (2017), "Preliminary understanding of CO_2 sequestration and enhanced methane recovery in Ranigang coalfield of India by reservoir simulation", *Energy Proc.*, **114**, 4643-4657.

De Borst, R., Réthoré, J. and Abellan, M.A. (2000), "A numerical approach for arbitrary cracks in a fluid-saturated medium", *Arch. Appl. Mech.*, **75**(10-12), 595-606.

Douglas Jr., J., Pereira, F. and Yeh, L.M. (2000), "A locally conservative Eulerian-Lagrangian method for flow in a porous medium of a mixture of two components having different densities", *Numer. Treat. Multiph. Flow. Por. Med.*, 138-155.

Ezekwe, N. (2010), *Petroleum Reservoir Engineering Practice*, Prentice-Hall, Bergen County, New Jersey, U.S.A.

Geiger, S., Schmid, K.S. and Zaretskiy, Y. (2012), "Mathematical analysis and numerical simulation of multi-phase multi-component flow in heterogeneous porous media", *Curr. Opin. Colloid & Interf. Sci.*, **17**(3), 147-155.

Hadzalic, E., Ibrahimbegovic, A. and Dolarevic, S. (2018), "Failure mechanisms in coupled soil-foundation systems", *Coupled Syst. Mech.*, **7**(1), 27-42.

Hadzalic, E., Ibrahimbegovic, A. and Nikolic, M. (2018), "Failure mechanisms in coupled poro-plastic medium", *Coupled Syst. Mech.*, **7**(1), 43-59.

Hanspal, N.S., Waghode, A.N., Nassehi, V. and Wakeman, R.J. (2009), "Development of a predictive mathematical model for coupled Stokes/Darcy flows in cross-flow membrane filtration", *Chem. Eng. J.*, **149**(1-3), 132-142.

Hoteit, H. and Firoozabadi, A. (2006), "Compositional modeling of discrete-fractured media without transfer functions by the discontinuous Galerkin and mixed methods", *SPE J.*, **11**(3), 341-352.

Hoyos, B. (2004), "Generalized liquid volume shifts for the Peng-Robinson equation of state for C_1 to C_8 hydrocarbons", *Lat. Am. Appl. Res.*, **34**(2), 83-89.

Jiang, J. and Younis, R.M. (2015), "A multimechanistic multicontinuum model for simulating shale gas reservoir with complex fractured system", *Fuel*, **161**, 333-344.

Jmili, A., Wilhite, G.P. and Green, D. (2011), "Modeling gas-phase mass transfer between fracture and matrix in naturally fractured reservoirs", *Soc. Petrol. Eng. J.*, **16**(4), 795-811.

Lake, W.L. (1989), *Enhanced Oil Recovery*, Prentice-Hall, Bergen County, New Jersey, U.S.A.

Lee, S.H., Jensen, C.L. and Lough, M.F. (2000) "Efficient finite-difference model for flow in a reservoir with multiple length-scale fractures", *SPE J.*, **5**(3), 268-275.

Lee, S.H., Lough, M.F. and Jensen, C.L. (2001) "Hierarchical modeling of flow in naturally fractured formations with multiple length scales", *Wat. Res. Res.*, **37**(3), 443-455.

Lewis, R.W. and Schrefler, B.A. (1998) *The Finite Element Method in the Static and Dynamic Deformation and Consolidation of Porous Media*, 2nd Edition, John Wiley & Sons, Chichester, England.

Li, L. and Yin, Z. (2017), "Numerical simulation of groundwater pollution problems based on convection diffusion equation", *Am. J. Comput. Math.*, **7**(3), 350-370.

Maes, J., Muggeridge, A.H., Jackson, M.D., Quintard, M. and Lapene, A. (2016), "Modelling in-situ upgrading of heavy oil using operator splitting method", *Comput. Geosci*., **20**(3), 581-594.

Mendes, M.A., Murad, M.A. and Pereira, F. (2012), "A new computational strategy for solving two-phase flow in strongly heterogeneous poroelastic media of evolving scales", *Int. J. Numer. Analy. Meth. Geomech.*, **36**(15), 1683-1716.

Moinfar, A. (2013), "Development of an efficient embedded discrete fracture model for 3D compositional reservoir simulation in fractured reservoirs", Ph.D. Dissertation, The University of Texas at Austin, Austin, Texas, U.S.A.

Nair, N., Bryant, S.L. and Jennings, J.W. (2008), "Finding the continuum scale in highly heterogeneous rocks: Example of a large touching vug carbonate", *Proceedings of the Society of Petroleum Engineers Annual Technical Conference and Exhibition*, Denver, Colorado, U.S.A., September.

Nelson, R. (2001), *Geologic Analysis of Naturally Fractured Reservoirs*, 2nd Edition, Gulf Professional Publishing, Houston, Texas, U.S.A.

Nikolic, M., Ibrahimbegovic, A. and Miscevic, P. (2016), "Discrete element model for the analysis of fluid-saturated fractured poro-plastic medium based on sharp crack representation with embedded strong discontinuities", *Comput. Meth. Appl. Mech. Eng.*, **298**, 407-427.

Saad, Y. (2003), *Iterative Methods for Sparse Linear Systems*, 2nd Edition, Society of Industrial and Applied Mathematics, Philadelphia, Pennsylvania, U.S.A.

Secchi, S. and Schrefler, B.A. (2012), "A method for 3-D hydraulic fracturing simulation", *Int. J. Fract.*, **178**(1-2), 245-258.

Souza, G. and Amaral Souto, H.P. (2016), “A comparative study of non-Darcy flows in naturally fractured gas reservoirs”, *J. Brazil. Soc. Mech. Sci. Eng.*, **38**(6), 1701-1715.

Tiab, D. and Donaldson, E.C. (2004), *Petrophysics*, Gulf Professional Publishing, U.S.A.

Vennemo, S. (2016), “Multiscale simulation of thermal flow in porous media", M.Sc. Dissertation, Norwegian University of Science and Technology, Trondheim, Norway.

Wang, C. (2013), “Pressure transient analysis of fractured wells in shale reservoirs", M.Sc. Dissertation, Colorado School of Mines, Golden, Colorado, U.S.A.

Wu, Y. and Sun, S. (2016), “Equivalence of two models in single-phase multicomponent flow simulations”, *Comput. Math. Appl.*, **71**(6), 1303-1316.

Zaydullin, R., Voskov, D.V., James, S.C., Henley, H. and Lucia, A. (2014), “Fully compositional and thermal reservoir simulation”, *Comput. Chem. Eng.*, **63**, 51-65.

Zidane, A. and Firoozabadi, A. (2017), “Fracture-cross-flow equilibrium in compositional two-phase reservoir simulation”, *SPE J.*, **22**(3), 1-21.

AI